Structural, electronic, optical and mechanical properties of InP alloyed with Zn, Si, Sn and S under pressure: First-principles calculation

Article *in* Journal of Alloys and Compounds · April 2017

DOI: 10.1016/j.jallcom.2017.01.063

CITATIONS
19

READS
196

3 authors:

Prayoonsak Pluengphon
Huachiew Chalermprakiet University
44 PUBLICATIONS **447** CITATIONS
SEE PROFILE

Thiti Bovornratanaraks
Chulalongkorn University
158 PUBLICATIONS **1,805** CITATIONS
SEE PROFILE

Udomsilp Pinsook
Chulalongkorn University
96 PUBLICATIONS **1,078** CITATIONS
SEE PROFILE

Structural, electronic, optical and mechanical properties of InP alloyed with Zn, Si, Sn and S under pressure: first-principles calculation

Prayoonsak Pluengphon[a,c,*], Thiti Bovornratanaraks[b,c,*], Udomsilp Pinsook[b,c]

[a]*Division of Physical Science, Faculty of Science and Technology, Huachiew Chalermprakiet University, Samutprakarn 10540, Thailand*

[b]*Extreme Conditions Physics Research Laboratory, Department of Physics, Faculty of Science, Chulalongkorn University, Bangkok 10330, Thailand*

[c]*ThEP Center, CHE, 328 Si-Ayuttaya Road, Bangkok 10400, Thailand*

*Corresponding Author Email: prayoonsak@gmail.com, thiti.b@chula.ac.th

Abstract

Structural, electronic, optical and mechanical properties of Zn, Si, Sn and S substitutions on InP supercell under pressure in zinc blende (ZB) and rock salt (RS) phases are presented using first-principles method. Cohesive energy and enthalpy difference are observed, and found that the order of possible spontaneous process in experimental growth, which introduced from enthalpy difference, is (In,Zn)P > In(P,S) > In(Si,P) > In(Sn,P). The lower enthalpy difference in RS structure indicates that the spontaneous process of impurity substitution can be occurred in RS more than in ZB. Phase transition from ZB to RS reduces the strain on crystal lattice by the increasing of chemical bond length. The chemical bonding of Zn-P in ZB is the strongest sharing electrons when compared with other compounds, Zn-P>Si-In>S-In>Sn-In. The dielectric performance of InP is reduced by the alloying effect, and it transforms to the conductor performance as high frequencies. Order of photo-absorption coefficient in range of visible light with the impurities is Sn>Si>S>Zn, and it reduces under high-pressure. Mechanical stability of InP alloys was observed, and satisfied the Born stability criteria. The impurities reduce Shear modulus of pure InP. Poisson's ratio of InP alloys in RS exhibit small deformation and high isotropy, corresponding to high-symmetry cubic phase. *B/G* ratio indicates that ductility of InP alloys is reduced, when it transformed to RS. The ductility of InP is induced by the alloying effect due to the *B/G* ratio increasing.

Keyword: Phase stability, Elastic properties, InP alloys, High pressure, Ab initio method

1. Introduction

During the last decades, the alloys and compounds of III-V binary semiconductors are great of interest for many applications on the electronic devices such as light emitting diodes, optoelectronic devices and photovoltaic materials. The efficiency of solar cell highly depends on the electronic and optical properties of the semiconductor materials in multilayer films. Indium Phosphide (InP) is one of most promising materials in a III-V group which used as a substrate for epitaxial growth

applied in photovoltaic multilayers [1-3]. InP is widely used in high-frequency and high-power electronic devices because it has superior electron velocities and long-lived optical phonons when compared with other III-V compounds [3, 4]. Stable crystal structure of InP at ambient pressure (0 GPa) is zinc blende (ZB) in space group *F-43m* [5-7], which related with most of III-V semiconductors such as GaAs, GaN, InAs and InSb. When high-pressure in order of gigapascal (GPa) presses on a primitive cell, the stable structure of InP has the transformations in each pressure range as *F-43m*→*Fm-3m*→*Cmcm*→*Immm*→*Pm-3m* at 5.6, 11.0, 50.0 and 102.0 GPa, respectively [7]. The 2nd phase of InP is rock salt (RS) phase in space group *Fm-3m*. The 1st transformation path from ambient phase to RS normally deforms to non-semiconductor due to the reconstruction bonding of disorder to order structures during phase transition that found in $CuGaSe_2$ [8,9] and GaAs [10,11]. High-pressure condition and structural phase transition have highly effected on chemical bond, band structure, electronic density of state (EDOS), photo absorption, elasticity and superconductivity [12-14]. Bouarissa studied high-pressure effects on the properties of InP, including electronic and optical properties [15], valence and conduction charge densities [16], and bonding and iconicity [17]. It was found that electronic charge densities are sensitive to the effect of hydrostatic pressure and the transverse effective charge decreases with increasing pressure which indicates the increased covalent bonding in the InP. In addition, the effects of impurity atoms on InP at ambient pressure have widely studied because the electronic and optical properties respond significantly with the concentration of impurities [18-23]. Zn-doped InP layers were obtained by *in situ* doping in low pressure metalorganic chemical vapor deposition, and thermal diffusion from a Zn-containing film [18]. Band edge peaks and band of shallow donor to acceptor transition peak were observed in *in situ* Zn-doped InP, implying that interstitial Zn atoms were generated during *in situ* doping. Schubert et al. [19] reported that Zn diffusion depends strongly on the concentration of Zn. Zn-doped is preferable in InP over other p-type dopants because it has high electrical activity, moderate diffusion, controllable incorporation and low residual toxicity. And then, the incorporation and doping process of Si, S and Zn impurities in InP by metalorganic vapor phase epitaxy have been studied both standard growth conditions and selective area growth conditions [20]. It was found that Zn-S co-doping shows a Zn dopant concentration enhancement in selective area growth conditions, while it remains constant in standard growth conditions. The Si concentration was unexpectedly independent of the growth rate in selective area growth conditions. Youssef [21] studied optical properties of Zn-doped InP, and found that Zn-doped increases refractive index and reduces band gap of InP.

From the literature review, we can see that the physical properties of both doped and undoped InP are widely studied at ambient pressure. However, high-pressure properties, including formation energies, free energy differences, electronic structures, optical properties and mechanical properties, on the InP with impurities are still incomplete. High-pressure technique is a vivid choice to change physical properties of condensed matters because it has high effect on atomic structures in scale of primitive cell. The electronic, optical and mechanical properties depend on the changed atomic structures under high-pressure. InP and their compounds are widely used in multilayer solar cell applications which ability of photovoltaic process based on

these properties. Therefore, the high-pressure properties of Zn, Si, Sn and S substituted on InP calculated from first-principles calculation are presented and discussed in this report.

2. Calculation details

The first-principles calculations based on density functional theory (DFT) are performed to solve the Kohn-Sham equations by self-consistent field method (SCF) [24] as implemented in Cambridge Serial Total Energy Package (CASTEP) code [25]. To study DFT calculations in the alloyed InP systems, the local density approximation schemes of Ceperley-Alder-Perdew-Zunger (LDA-CAPZ) and the generalized-gradient approximation functional of Perdew-Burke-Ernzerhof (GGA-PBE) [26, 27] are compared at ambient condition for finding the suitable exchange-correlation functional term in Kohn-Sham equations. In table 1, we can see that lattice parameters and bulk modulus of InP calculated from LDA-CAPZ functional are better than GGA-PBE results; therefore, LDA-CAPZ is mainly used as exchange-correlation functional for finding the high-pressure properties of the alloyed InP systems. This supported the DFT results in ZB structure (in figure 1) of GaAs (III-V) semiconductor in previous work [11].

Table 1: Lattice parameters (a=b=c), volume cell (V) and bulk modulus (B_0) at 0 GPa in *ZB* structure of InP compared with previous studies [3, 6].

a (Å)	V (Å^3)	B_0 (GPa)	Method	Ref.
5.968	212.6	59.3	GGA-PBE	This work
5.832	198.4	71.8	LDA-CAPZ	This work
5.869	202.2	71.0	EPM	[3]
5.856	200.8	71.1	Experiment	[6]

To study the InP alloys, the impurity atoms which consist of Zn, Si, Sn and S are substituted on In (or P) site in 1/8 of InP with super cell size 2×2×2 as shown in figure 1(c) and 1(d). The maximum energy of plane wave basis set used at 450 eV, which is suitable cutoff energy to cooperate with ultrasoft-pseudopotential [28]. Monkhorst-Pack grid sizes [29] for 2×2×2 super cells both ZB and RS structures are 8×8×8, while k point in undoped InP initially finites as the condition of $1/k \approx 0.035$. The Brodyden-Fletcher-Goldfarb-Shanno (BFGS) [30] minimization scheme is used in geometry optimization. External forces and pressure tensors on optimized structures are controlled by Hellmann-Feynman theorem [31]. The BFGS optimization was considered to be completed when the total energy difference was less than 2×10^{-6} eV/atom, Hellman–Feynman forces were less than 0.006 eV/Å, the maximum ionic displacement within 0.0002 Å, and all of the stress components within 0.003 GPa. The average isotropic moduli in bulk obtained from elastic constants by Voigt-Reuss-Hill (VRH) method [32, 33].

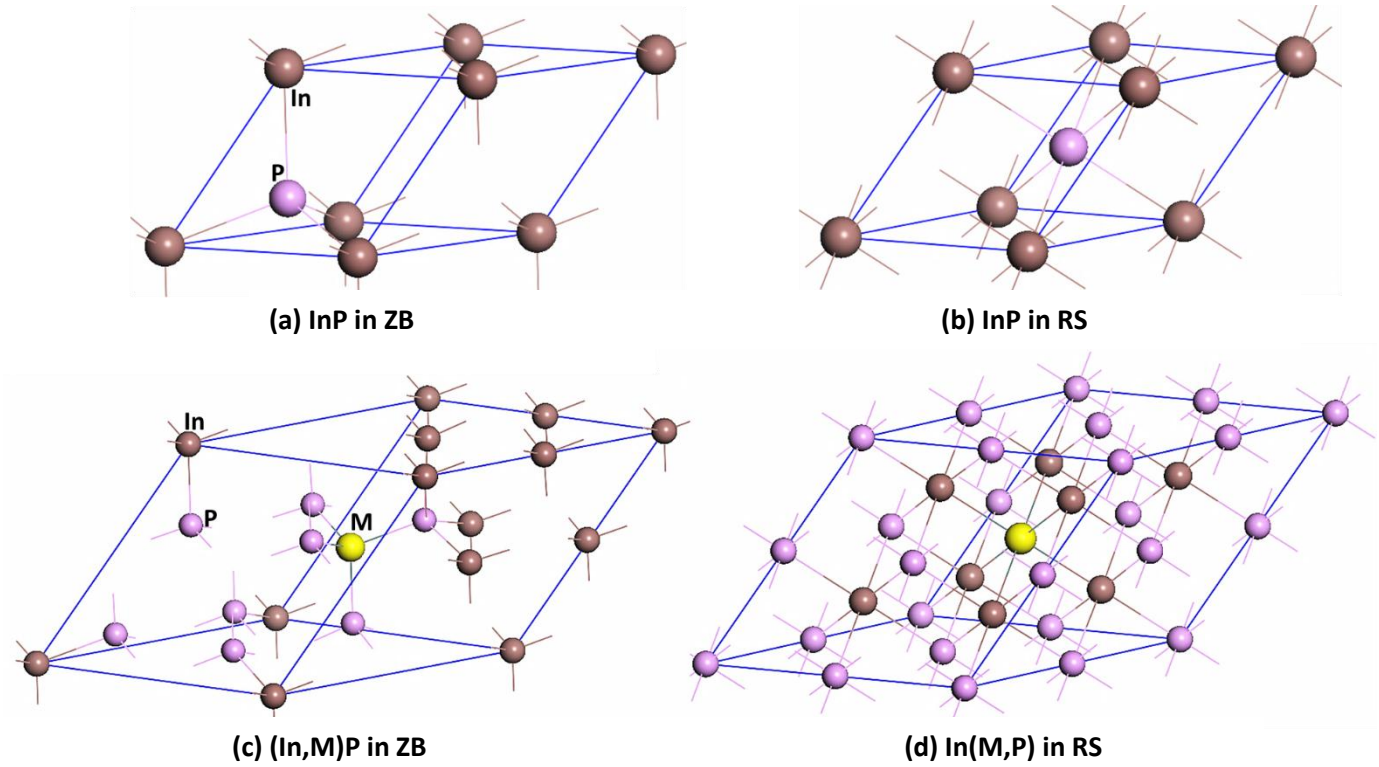

Figure 1: Atomic structures of InP in pure and alloys conditions (a) InP in ZB structure (b) InP in RS structure (c) InP replaced by M atom in ZB supercell (d) InP replaced by M atom in RS supercell.

3. Results and discussion

3.1 Site preference and phase stability

In order to understand the structural features of the InP alloys, it is investigated by considerations the cohesive energy (E_{coh}), which is a measure of the strength of atomic forces in solid state. The cohesive energy can be obtained from the difference between the average energy of the free atoms and that of a solid, which is correlated with the structural stability in ground state. The cohesive energy per formula unit (eV/f.u.) of the compounds $In_{1-x}M_xP$ or (In,M)P can be calculated in form [34]

$$E_{coh} = (1-x)E_{atom}^{In} + xE_{atom}^{M} + E_{atom}^{P} - E_{total}^{(In,M)P}$$

While cohesive energy per formula unit of the compound InM_xP_{1-x} or In(M,P) is

$$E_{coh} = E_{atom}^{In} + xE_{atom}^{M} + (1-x)E_{atom}^{P} - E_{total}^{In(M,P)}$$

where $E_{total}^{(In,M)P}$ and $E_{total}^{In(M,P)}$ are the total energies per formula unit of the (In,M)P and In(M,P) compounds, E_{atom}^{In}, E_{atom}^{M} and E_{atom}^{P} are the energies of In, M and P of isolated constituent atoms (M =Zn, S, Si and Sn). The cohesive energies at ambient pressure are analyzed as shown in table 2. We also compare Gibbs's free energy of system ($G=E+PV-TS$) which $G=E+PV=H$ at $T=0$ K. The free energy differences ($H-H_0$) can be obtained from free energies of the alloyed InP compounds (H) based on that of pure InP (H_0).

Table 2: Comparisons cohesive energy and free energy difference of InP alloys at 0 GPa.

compound	InP	(In,Zn)P	In(P,S)	(In,Si)P	In(Si,P)	(In,Sn)P	In(Sn,P)
E_{coh} (eV/f.u.)	8.58	8.32	8.34	8.72	8.32	8.54	8.14
H-H_0 (eV/f.u.)	0.00	-18.52	-12.24	181.86	9.28	183.34	10.76

The results supported well-kwon knowledge that site preference of Zn (II-B) impurity is the In site, while S (VI-A) atom prefers to substitute on P site, depending on position of elements and electronegativity values in periodic table. The positive cohesive energies of (In,Zn)P and In(P,S), which are 8.32 and 8.34 eV/f.u., show the structural stability in solid form of the InP alloys. When we compare free energies of alloys based on pure InP, the negative free energies (H-H_0<0) supported stability of (In,Zn)P and In(P,S) compounds. It is indicated that the Si and Sn impurities (IV-A group) prefer to substitute on the super cell of InP in the forms of In(Si,P) and In(Sn,P). Therefore, site preferences of alloying InP with Zn, S, Si and Sn are (In,Zn)P, In(P,S), In(Si,P) and In(Sn,P), respectively. The possible spontaneous process in experimental growth can be suggested from H-H_0 which is (In,Zn)P > In(P,S) > In(Si,P) > In(Sn,P) as shown in table 2.

Table 3: Free energy differences of the (In,Zn)P, In(P,S), In(Si,P) and In(Sn,P) alloys based on InP in ZB and RS phases under pressure 0, 5 and 10 GPa.

Structure	P (GPa)	H_{InP} (eV/f.u.)	H-H_{InP} (eV/f.u.)			
		InP	(In,Zn)P	In(Si,P)	In(Sn,P)	In(P,S)
ZB	0	-1740.80	-18.52	9.28	10.76	-12.24
	5	-1739.20	-18.58	9.28	10.82	-12.20
	10	-1737.68	-18.62	9.30	10.86	-12.18
RS	5	-1738.84	-18.74	6.18	7.48	-12.56
	10	-1737.60	-18.78	6.10	7.44	-12.56

To compare the possible spontaneous process in ZB and RS phases, free energies of the (In,Zn)P, In(Si,P), In(Sn,P) and In(P,S) compounds under pressure are observed and compared with InP as shown in table 3. The calculated phase transition from ZB to RS occurred at 10-12 GPa that are in consistent with previous works [1, 7]. The effect of impurity has small effect on the transition pressure [35]. We found that the increasing of pressure in ZB from 5 to 10 GPa has small effect on $\Delta H = H - H_{InP}$, while it reduces significantly during phase transformation from ZB to RS in all alloys. The lower ΔH in RS indicates that the spontaneous process of impurity substitution can be occurred in RS more than in ZB.

3.2 Electronic properties

The EDOSs of (In,Zn)P, In(Si,P), In(Sn,P) and In(P,S) are analyzed to understand the effects of high-pressure and phase transition on the InP alloys in ZB and RS. In figure 2(a), we found that band gap of InP appears only in ZB phase (0, 5 and 10 GPa), where Fermi level is set at zero energy and denoted by the vertical dash-line. But the gap is vanished in RS structure both 5 and 10 GPa. The closed band gap occurred due to the difference of chemical bonds and number of neighbor atoms in ZB and RS. It is well known that high-pressure effect can change structure of InP from ZB to RS, and semiconductor properties (in ZB) will be changed to non-semiconductor (in RS) [1,7]. The peaks near valence band maximum (VBM) and conduction band minimum (CBM) are observed in figure 2(b). It is seen that the alloying with Si and Sn reduce band gap of InP, and generate the impurity peak at VBM. The EDOSs of (In,Zn)P in figure 2(c) indicate that the peaks at VBM and CBM in ZB phase are reduced when pressure increases, and the energy gap still disappears in RS phase. For comparisons of alloying with S, Si and Sn as shown in figure 2(d), 2(e) and 2(f), we found that the peaks of EDOSs at VBM and CBM under the increasing of pressure are reduced and spread out in x-axis. EDOSs of In(Sn,P) and In(Si,P) appear new peak at VBM, while it is not found in In(P,S). Available states of EDOSs at 5 and 10 GPa are extended along energy-axis because the carriers receive the stimulated energies from the external forces or high-pressure. Partial density of states (PDOSs) of InP alloys are presented in figure 3, and found that *p*-orbital is mainly as available states in all alloys. The Si and Sn, which are impurities in IV-A group, gave similar distribution of PDOS. VBM of In(Si,P) and In(Sn,P) had shifted on the right-hand side compared with Fermi level, while PDOS of S has shifted in the opposite way. PDOS of Zn atom shows *s*, *p* and *d* orbitals of the transition element. The *p*-orbital of Sn at VBM and CBM reduced under high-pressure in ZB which related with EDOS. It has shifted in right-hand side, and the gap is closed in RS. The population analysis indicates that Zn atom in InP gave the *p*-*d* hybridization, while Si, S and Sn atoms gave the hybridization of *s*-*p*. To understand the chemical bonding and electron sharing between impurity and nearby atoms, the electron density differences are investigated in figure 4. The electron density difference that indicates electron delocalization in solid can be obtained from the difference between the self-consistent valence charge density and the superposition of atomic valence densities. It is useful for illustrating how chemical bonds are formed across the whole system as the electron density difference can help identifying the types of chemical bonds. Contour plot divides the gradient of electron density difference between Blue zone = -0.15 and Red zone = +0.15. Strength of In-P bond in ZB phase increases slowly under the increasing pressure (0, 5 and 10 GPa) which related with previous work [16], shown in figure 4(a), 4(b) and 4(c). But it is seen that structural phases of InP is relaxed when transforms to RS phase in figure 4(d). Although the volume cell is reduced by phase transition from ZB to RS, the covalent bond of In-P is weakened in RS phase due to the increasing of bond length 2.630 Å that larger than in ZB (2.435 Å). The increasing of bond length under volume reducing in InP system is occurred because it is trying to reduce the stress and strain on lattice by phase transition. The sharing of electron density In-P in RS is related to the bond length increasing as shown in table 4. For InP alloyed with elements, order of strong covalent bonding is Zn-P>Si-In>S-In>Sn-In, while bond length as the

same pressure is In-Sn>In-S>In-Si>In-P>Zn-P. The bond length in ZB phase decreases under high-pressure, and electron density difference indicates the strong of bond at 10 GPa which supported N. Bouarissa's work [17]. The contour plots showed that Zn-P bond in (In,Zn)P-ZB has the strongest sharing electrons which related to the shortest bond length.

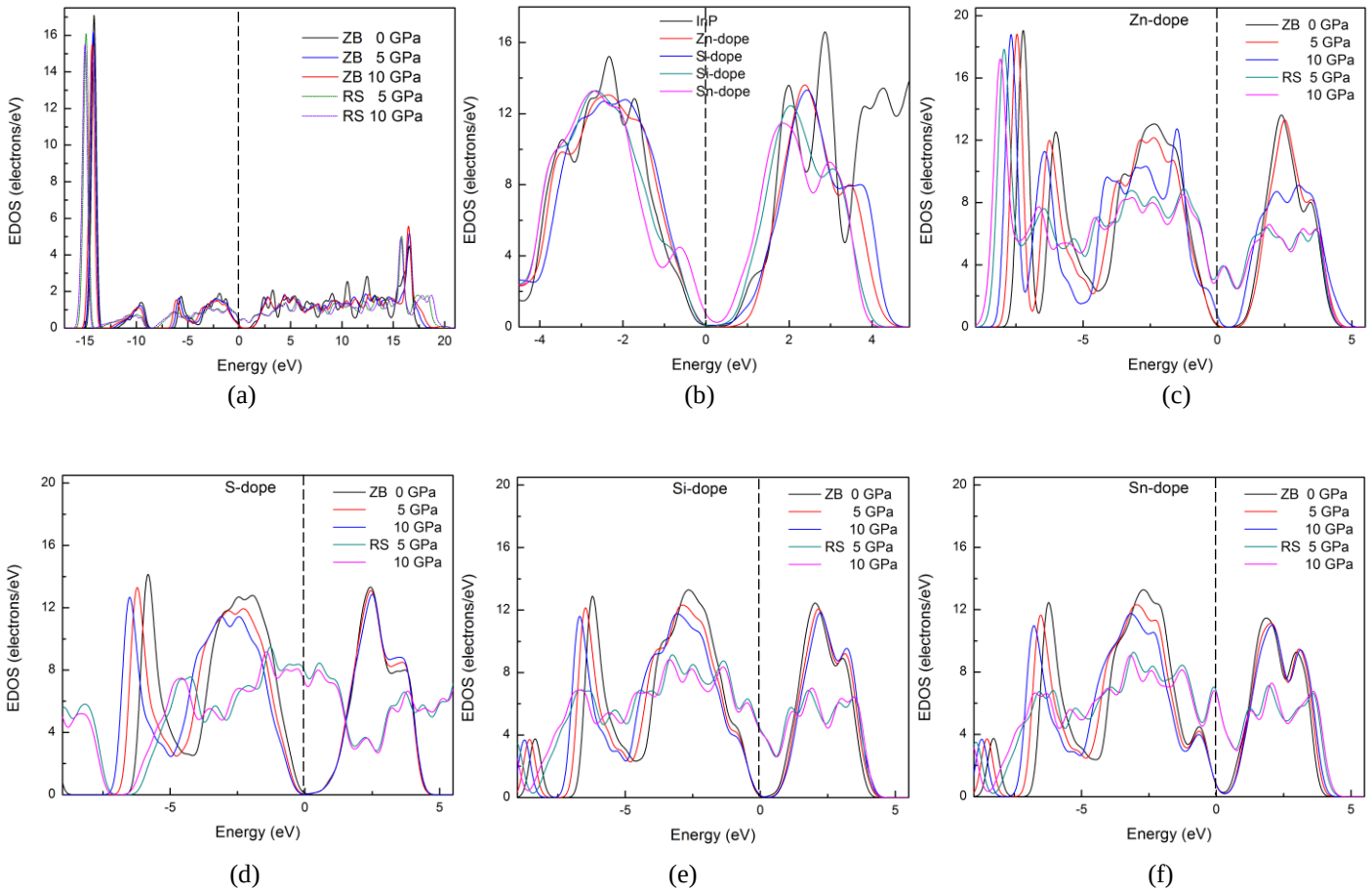

Figure 2: Comparisons total density of states of (a) pure InP in ZB (0, 5 and 10 GPa) and RS (5 and 10 GPa), (b) InP alloys (0 GPa), (c) (In,Zn)P, (d) In(P,S), (e) (In,Si)P and (f) Sn in InP under pressure in ZB and RS.

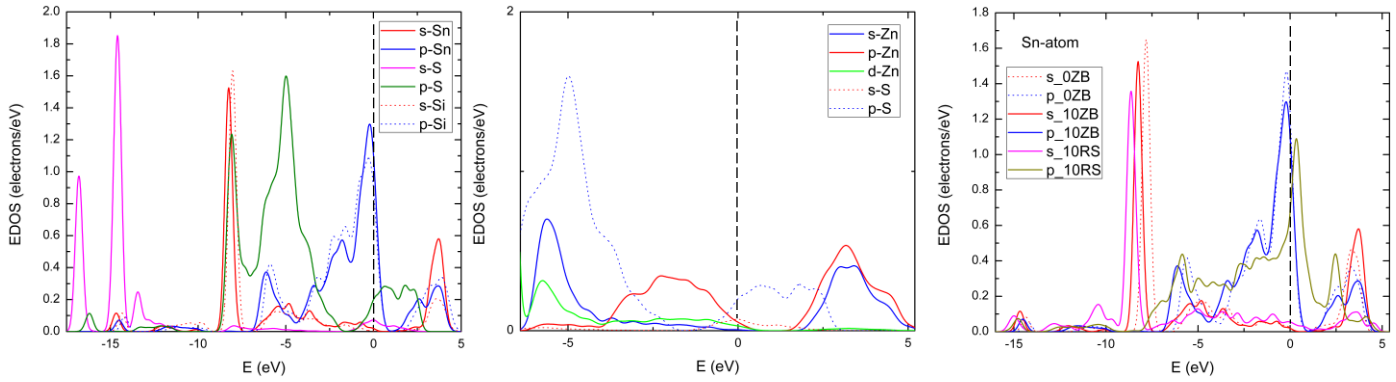

Figure 3: Partial density of states of impurity atoms (a) *s* and *p* orbitals of Sn, S and Si at 0 GPa. (b) *s*, *p*, *d* orbitals of Zn and S at 0 GPa. (c) *s* and *p* orbitals of Sn-atom in ZB (0 and 10 GPa) and RS (10 GPa).

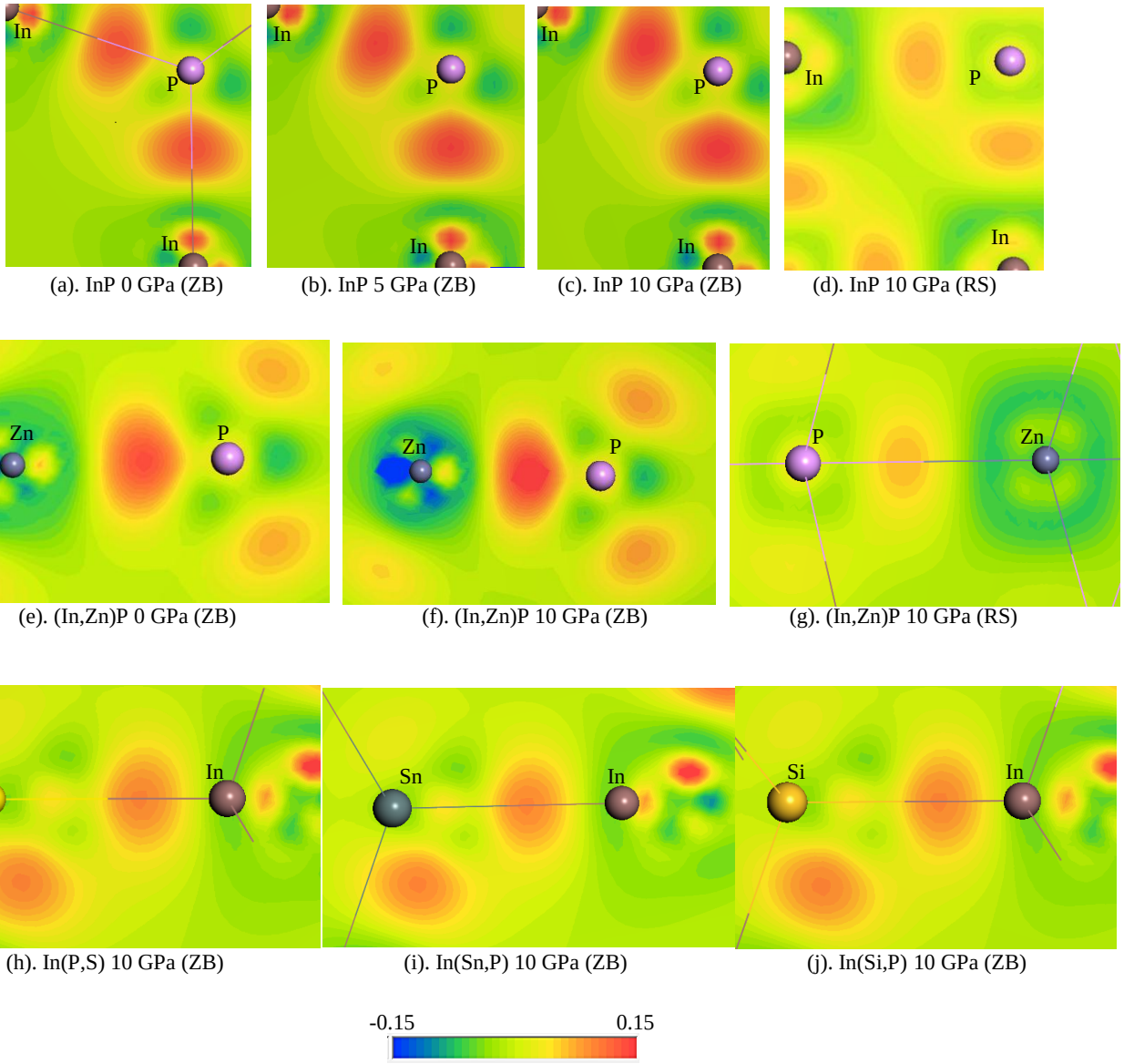

(a). InP 0 GPa (ZB) (b). InP 5 GPa (ZB) (c). InP 10 GPa (ZB) (d). InP 10 GPa (RS)

(e). (In,Zn)P 0 GPa (ZB) (f). (In,Zn)P 10 GPa (ZB) (g). (In,Zn)P 10 GPa (RS)

(h). In(P,S) 10 GPa (ZB) (i). In(Sn,P) 10 GPa (ZB) (j). In(Si,P) 10 GPa (ZB)

Figure 4: Electron density difference between two atoms of InP and their alloys under pressure.

Table 4: Bond lengths between two atoms in the alloys and pure of InP under pressure.

Structure	*P* (GPa)	Bond length (Å)				
		In-P	Zn-P	In-Si	In-Sn	In-S
ZB	0	2.525	2.354	2.532	2.657	2.582
	5	2.474	2.295	2.479	2.602	2.531
	10	2.435	2.249	2.436	2.563	2.495
RS	5	2.668	2.542	2.705	2.801	2.708
	10	2.630	2.505	2.664	2.757	2.671

3.3 Optical properties

The optical properties are also investigated so that photoabsorption of the InP alloys under pressure will be compared and suggested the suitable condition for photo-application. Probability transition states of carriers from valence band to conduction band related to dielectric function, which the external photo energy is translated to the excited energy of intrinsic and extrinsic carriers. Real and imaginary parts of dielectric functions, which are the basic parameters to obtain all optical properties, are presented, and compared with the experiment in range of energies 0.5-6.0 eV [36] as shown in figure 5(a). The calculated dielectric functions shifted in low frequency (-x axis) when compared with experiment (dot line) because of the lower pseudogap from calculation with LDA. However, the trends of two graphs are in consistent with experiment [36]. The calculated dielectric functions of (In,Zn)P in figure 5(b) are smooth functions more than in InP. At high-pressure (10 GPa), the imaginary part of (Zn,In)P has shifted to the positive frequency (+x axis) which is consistent with previous work [15]. At low frequencies range 0-2 GPa, the imaginary part is dominated as $\varepsilon_2 > \varepsilon_1$. The dielectric performance is reduced by the alloying elements due to the reducing of $\varepsilon_2 / \varepsilon_1$ ratio, and it transforms to conductor performance as high frequencies.

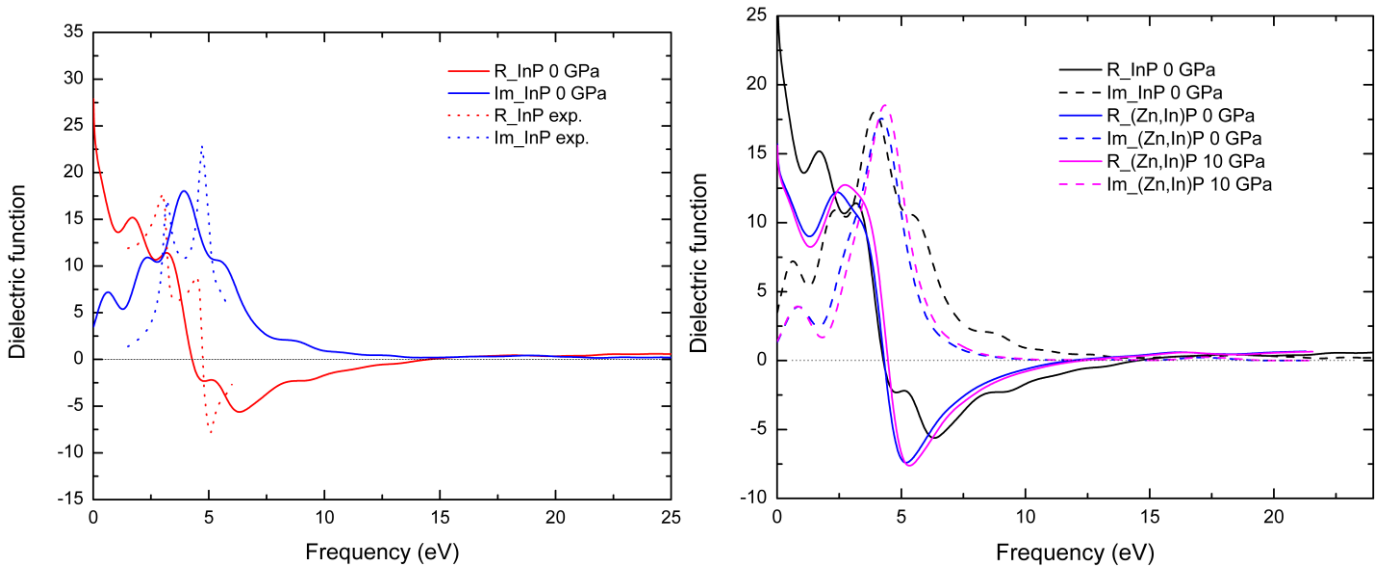

(a) (b)

Figure 5: The calculated dielectric functions in real (R) and imaginary (Im) parts (a) comparison with previous experiment [36] (b) comparison between InP and (In,Zn)P at 0 and 10 GPa.

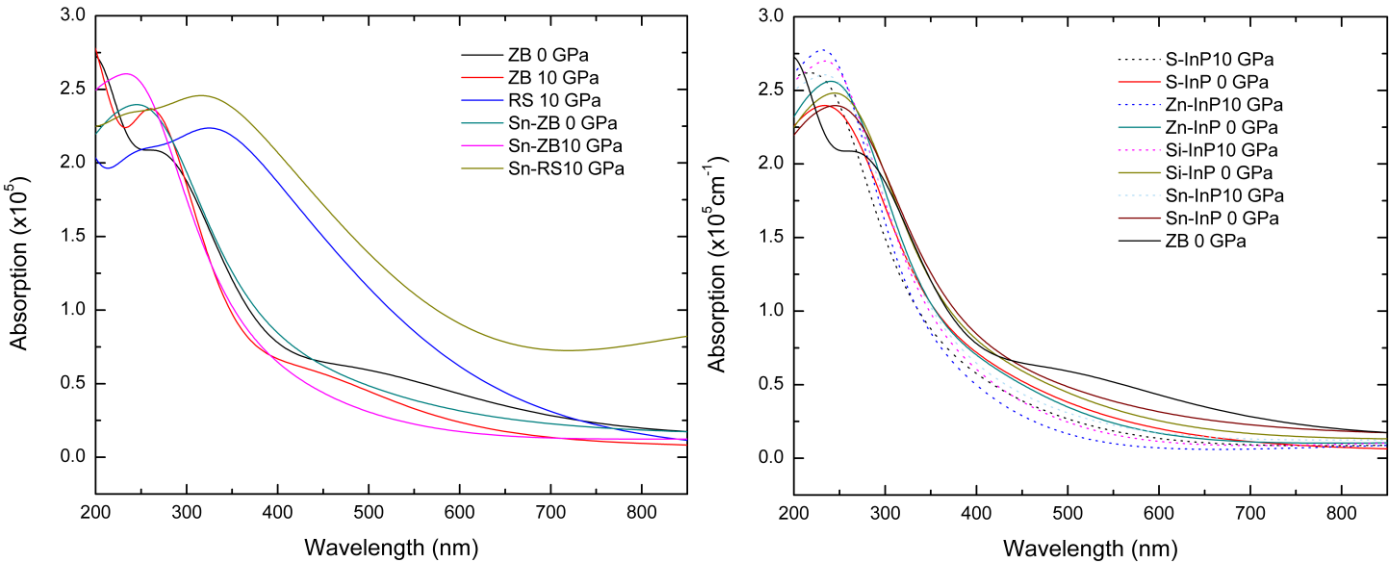

(a) (b)

Figure 6: Photoabsorptions of (a) InP and In(P,Sn) in ZB and RS. (b) (Zn,In)P, In(P,S), In(Si,P), In(Sn,P) and InP in ZB at 0 and 10 GPa.

Photoabsorption can be obtained from the dielectric function through the Kramers–Kronig relations [37]. Photo absorption in wavelength between 200-850 nm (in range of ultraviolet, visible light and infrared) is given in figure 6. We found that high-pressure in ZB phase gives unsuitable condition for photoabsorption of InP alloys. Absorption coefficient of the InP alloys in ZB phase decreases under the increasing pressure, while it increases in RS phase. However, the InP alloys had become the non-semiconductor due to the closed band gap. The photoabsorptions generally focus on the semiconductor phase (ZB) that the carrier transition through band gap. In figure 6(b), we can see that absorption coefficients of the InP alloys are lower than of pure condition. Order of absorption coefficient of InP-ZB with impurities is Sn>Si>S>Zn, and it decreases at high pressure (10 GPa). Photoabsorptions in ZB are normally reduced under high pressure due to the increasing band gap and the decreasing peaks of EDOSs at VBM and CBM.

3.4 Mechanical properties

Elastic constants are calculated to investigate the mechanical properties of the alloying conditions of InP under pressure. The elastic constants (c_{ij}) can provide the hardness, stress and strain in each direction of external forces on a primitive cell of material. The calculated elastic constants of InP with the LDA-CAPZ, GGA-PBE and GGA-PBEsol functionals are compared with the previous experiment [6] as shown in table 5. We can see that the LDA-CAPZ result is in good agreement with previous experiment [6], better than PBE and PBEsol. The calculated elastic stiffness constants are satisfied the Born stability criteria in conditions of cubic system (both ZB and RS) [38, 39]: $c_{11}+2c_{12}>0,\ c_{44}>0,\ c_{11}-c_{12}>0.$

Table 5: The calculated elastic properties (in GPa unit) by varying functionals compared with experiment results of InP at 0 GPa.

Method	c_{11}	c_{12}	c_{44}	B	G	Y	e
GGA-PBE	86.8	45.5	42.0	59.3	31.5	55.5	0.344
GGA-PBEsol	93.4	51.6	43.1	65.5	32.2	56.6	0.356
LDA-CAPZ	100.6	55.9	46.2	70.8	34.5	60.7	0.357
Exp. [6]	101	56	45	71	22.5	61	0.360

Bulk modulus (B), Shear modulus (G), Young's modulus (Y) and Poisson's ratio (ν) can be obtained from c_{ij} based on VRH method [32, 33]. The upper and lower bounds of the averages B and G in VRH scheme are B_V, B_R and G_V, G_R, respectively. For ZB and RS structures in cubic system [40],

$$B_V = B_R = (1/3)(c_{11}+2c_{12}),$$
$$G_V = (1/5)(c_{11}-c_{12}+3c_{44}),$$
$$G_R = 5(c_{11}-c_{12})c_{44}/(3c_{11}-3c_{12}+4c_{44}).$$

The bulk values (B, G, Y and ν) are estimated by VRH approximation:

$$B = (B_V + B_R)/2,$$
$$G = (G_V + G_R)/2,$$
$$Y = 9BG/(3B+G),$$
$$\nu = (3B-2G)/(6B+2G).$$

From the calculated B and G moduli, Chen et al. [41] proposed that Vickers hardness of polycrystalline materials can be estimated in terms of $k = \frac{G}{B}$ and G in the form

$$H_V = 2\left(k^2 G\right)^{0.585} - 3.$$

Nevertheless, Tian et al. [42] suggested that it may make the negative hardness for some low hardness materials due to the constant term ''-3'', so they modified new equation which can always give positive values for low hardness materials. Tian et al.'s correction which used in this work is

$$H_V = 0.92k^{1.137}G^{0.708}.$$

Table 6: Elastic parameters in a unit GPa (except ε) of InP and their alloys in ZB and RS structures.

Structure	condition	c_{11}	c_{12}	c_{44}	B	G	Y	ε	B/G	H_V
ZB	InP	100.6	55.9	46.2	70.8	34.5	60.7	0.36	2.05	4.99
0 GPa	(In,Zn)P	87.6	63.0	30.6	71.2	21.2	57.1	0.42	3.36	2.02
	In(P,S)	86.7	51.6	32.8	63.3	25.5	46.3	0.37	2.48	3.24
	In(Si,P)	82.3	60.4	23.8	67.7	17.4	56.1	0.42	3.89	1.48
	In(Sn,P)	75.2	59.6	16.7	64.8	12.3	56.6	0.44	5.27	0.82
10 GPa	InP	139.1	100.5	44.4	113.4	31.8	54.9	0.42	3.56	2.51
	(In,Zn)P	125.2	108.1	23.8	113.8	15.6	103.3	0.46	7.29	0.67
	In(P,S)	124.3	99.3	28.7	107.6	20.6	93.9	0.44	5.22	1.20
	In(Si,P)	121.4	106.8	19.6	111.7	13.2	102.9	0.47	8.46	0.50
	In(Sn,P)	114.0	105.1	10.1	108.0	7.3	103.2	0.48	14.79	0.18
RS	InP	269.4	64.2	66.2	132.6	79.0	244.7	0.19	1.68	11.25
10 GPa	(In,Zn)P	264.2	76.1	24.1	138.8	43.2	110.0	0.22	3.21	3.51
	In(P,S)	251.2	74.1	30.0	133.1	47.1	101.7	0.23	2.83	4.32
	In(Si,P)	229.6	78.2	29.0	128.7	43.1	99.9	0.25	2.99	3.81
	In(Sn,P)	224.2	73.1	23.2	123.5	38.1	103.6	0.36	3.24	3.18

The elastic parameters are shown in table 6 that the errors of c_{ij} calculations are less than 1 GPa. There are satisfied the Born stability criteria in all conditions [38, 39]. This indicates that structures of InP alloys are mechanically stable phases in ZB and RS. At ambient pressure, almost of *B*, *Y* and *S* of the InP alloys are smaller than of pure InP, especially the reducing of *S*. The critical *B/G* ratio of 1.75 separates type of ductile (>1.75) and brittle (<1.75) materials, which was introduced by Pugh [43]. While, Frantsevich et al. [44] suggested another critical ratio of B/G =2.67. Therefore, high-value of the *B/G* ratio indicates ductility of material. When compare between pure and alloyed conditions at a given pressure, almost c_{11} are decreased by alloying elements, while c_{12} are increased. Therefore, the substitutions with Zn, S, Si and Sn can change the properties of InP to ductile material. The value of *Y* indicates ability of resistance from the external tensile-strength that *Y* of the alloyed conditions increases in ZB (10 GPa) but it reduces in RS at 10 GPa, when compared with ambient pressure. This supported that RS is high symmetry structure which gave high resistance from the perpendicular forces. The parameters of c_{11}, c_{12} and *B* in ZB are increased under high-pressure because of the reducing of bond length and primitive cell. High Poisson's ratio (>0.25) [45, 46] corresponds to the large deformation of volumetric change and high anisotropy as shown in ZB phase. While, Poisson's ratio of

InP alloys in high-symmetry RS phase exhibit small deformation supported the higher isotropy, corresponding to high-symmetry cubic phase. High values of *B*, *G* and *Y* in RS in RS supported the packed atoms in high-symmetry system that it reduces the tangential stress. The *B/G* ratio in RS is lower than in ZB, indicating that ductility of InP alloys are reduced in RS. The estimated Vickers hardness from Tian et al.'s correction is listed in table 6. We can see that H_v of InP-ZB at ambient condition is 4.99 GPa, which is in good agreement with the experiment result (5.4 GPa) [41]. Tendency of H_v indicates that all impurities reduce hardness of pure InP. H_v decreases in ZB phase at high pressure (10 GPa) but it increases when transform to RS phase (H_v =11.25 GPa). The results of Vickers hardness in all compounds supported that RS phase is high symmetry structure because there are increased at the transition pressure of ZB-RS.

4. Conclusions

First-principles study on structural, electronic, optical and mechanical properties of Zn, Si, Sn and S substituted in InP supercell in ZB and RS structures are reported. Cohesive energy and enthalpy are observed, and indicated that In site is a preference site of Zn-alloyed, while a preference site of Sn, Si and S elements in InP is the P site. The possible spontaneous process in experimental growth which is introduced from H-H_0 is (In,Zn)P > In(P,S) > In(Si,P) > In(Sn,P). The lower ΔH in RS structure indicates that the spontaneous process of impurity substitution can be occurred in RS more than in ZB. For electronic structure, the *p*-orbital is mainly in available states in all compounds. Phase transition from ZB to RS reduces the strain on crystal lattice by the increasing of chemical bond length. The chemical bonding of Zn-P in ZB is the strongest sharing electrons when compared with other compounds, Zn-P>Si-In>S-In>Sn-In. For optical properties, the dielectric performance compared from $\varepsilon_2 / \varepsilon_1$ ratio is reduced by the alloying effect, and it transforms to conductor performance at high frequencies. Effect of impurities on ability of photo-absorption in range of visible light is Sn>Si>S>Zn, and it reduces as the pressure increasing. Mechanical stability of InP alloys was observed, and satisfied the Born stability criteria. The impurities reduce Shear modulus of pure InP. Poisson's ratio of InP alloys in RS exhibit small deformation and high isotropy, corresponding to high-symmetry cubic phase. High values of *B*, *G* and *Y* in RS supported atomic structure in RS that packed in high-symmetry system. *B/G* ratio indicates that ductility of all alloys in RS is reduced, when compared with ZB. The ductility of InP is induced by the alloying effect due to the *B/G* ratio increasing. High value of Vickers hardness in RS phase of all compounds supported that RS is high symmetry structure.

Acknowledgments

P. Pluengphon would like to thank the financial support from Thailand Research Fund (TRF) ID code TRG5880006, and Faculty of Science and Technology, Huachiew Chalermprakiet University. This work has been partially supported by National Research Council of Thailand. Computing facilities have been supported by Super SCI-II research grant, Faculty of Science and Ratchadaphiseksomphot Endowment Fund of Chulalongkorn University (CU-59-039-AM).

References

1. G.J. Ackland, Rep. Prog. Phys. 64 (2001) 483.

2. I. Vurgaftman, J.R. Meyer, L.R. Ram-Mohan, J. Appl. Phys. 89 (2001) 5815.

3. N. Bouarissa, Physica B 406 (2011) 2583.

4. P.L. Souza, P.R. Ribas, J.V. Bellini, W.M. Mendes, J. Appl. Phys. 79 (1996) 3482.

5. C.S. Menoni, I.L. Spain, Phys. Rev. B 35 (1987) 7520.

6. D.N. Nichols, D.S. Rimai, R.J. Sladek, Sol. Stat. Comm. 36(8) (1980) 667.

7. A. Mujica, R.J. Needs, Phys. Rev. B 55 (1997) 9659.

8. H. Xue, F. Tang,W. Lu, Y. Feng, Z.Wang, Y.Wang, Comput. Mater. Sci. 67 (2013) 21.

9. P. Pluengphon, T. Bovornratanaraks, Sol. Stat. Comm. 218 (2015) 1.

10. M. Durandurdu, D.A.Drabold, Phys.Rev.B:Condens.Matter 66 (2002) 045209.

11. P. Pluengphon, T. Bovornratanaraks, S. Vannarat, U. Pinsook, Solid State Commun. 195 (2014) 26.

12. Y. Zhao, H. Hou, Y. Zhao, P. Han, J. Alloys Compd. 640 (2015) 233.

13. J. Long, C. Shu, L. Yang, M. Yang, J. Alloys Compd. 644 (2015) 638.

14. Y. Xu, C. Chen, S. Wang, X. Sun, J. Alloys Compd. 669 (2016) 101.

15. N. Bouarissa, Solid-State Electronics 44 (2000) 2193.

16. N. Bouarissa, Materials Chemistry and Physics 65 (2000) 107.

17. N. Bouarissa, Infrared Physics & Technology 40 (1999) 117.

18. Y. Moon, S. Si, E. Yoon, S.J. Kim, J. Appl. Phys. 83 (1998) 2261.

19. E.F. Schubert, C.J. Pinzone, M. Geva, Appl. Phys. Lett. 67(5) (1995) 700.

20. J. Decobert, D. Herrati, V. Colson, D. Leclerc, L. Goldstein, J. Crystal Growth 248 (2003) 390.

21. S.B. Youssef, Physica A 235 (1997) 334.

22. H. Hu, X. Wu, R. Wang, Z. Jia, W. Li, Q. Liu, J. Alloys Compd. 666 (2016) 185.

23. Y. Hu, S. Shang, Y. Wang, et al., J. Alloys Compd. 671 (2016) 267.

24. M.C. Payne, M.P. Teter, D.C. Allan, T.A. Arias, D. Joannopoulos, Rev. Mod. Phys. 64 (1992)1045.

25. M.D. Segall, P.L.D. Lindan, M.J. Probert, C.J. Pickard, P.J. Hasnip, S.J. Clark, M.C. Payne, J. Phys.: Condens. Matter 14 (2002) 2717.

26. J.P. Perdew, J.A. Chevary, S.H.Vosko, K.A. Jackson, M.R.Pederson, D.J. Singh, C. Fiolhais, Phys. Rev. B 46 (1992) 6671.

27. J.P. Perdew, K. Burke, M. Ernzerhof, Phys. Rev. Lett. 77 (1996) 3865.

28. D. Vanderbilt, Phys. Rev. B 41 (1990) 7892.

29. H.J. Monkhorst, J.D. Pack, Phys. Rev. B 13 (1976) 5188.

30. B.G. Pfommer, M. Cote, S.G. Louie, M.L. Cohen, J. Comput. Phys. 131 (1997) 233.

31. R.P. Feynman, Phys. Rev 56 (4) (1939) 340.

32. R. Hill, Proc. Phys. Soc. A 65 (1952) 349.

33. G.V. Sinko, N.A. Smirnov, J. Phys.: Condens. Matter 14 (2002) 6989.

34. L. Li, Q. Gao, G. Lei, H. Xie, J. Deng, Xian-Ru Hu, J. Phys. Chem. Solids 94 (2016) 30–36.

35. P. Pluengphon, T. Bovornratanaraks, S. Vannarat,U. Pinsook, J. Phys.: Condens. Matter 24 (2012) 095802.

36. D.E. Aspnes, A.A. Studna, Phys. Rev. B 27 (1983) 985.

37. R.F. Egerton (1996). Electron energy-loss spectroscopy in the electron microscope (2nd ed.). New York: Plenum Press. ISBN 0-306-45223-5.

38. B.B. Karki, G.J. Ackland, J. Crain, J. Phys.: Condens. Matter 9 (1997) 8579.

39. F. Mouhat, F.X. Coudert, Phys. Rev. B 90 (2014) 224104.

40. X. Zhang, W. Jiang, J. Alloys Compd. 663 (2016) 565.

41. X.Q. Chen, H. Niu, D. Li, Y. Li, Intermetallics 19 (2011) 1275.

42. Y.J. Tian, B. Xu, Z.S. Zhao, Int. J. Refract. Met. Hard Mater. 33 (2012) 93.

43. S.F. Pugh, Philos.Mag. 45 (1953) 833.

44. I.N. Frantsevich, F.F.Voronov, S.A.Bokuta, Elastic Constants and Elastic Moduli for Metals and Insulators Handbook, Naukova Dumka, Kiev (1983).

45. S. Aydin, M. Simsek, J. Alloys Compd. 509 (2011) 5219.

46. C. Li, K. Zhang, J. Ru, J. Alloys Compd. 647 (2015) 573.